Investigations of Atmospheric Extinction Using Direct Solar Radiation Measurements Made with a Multiple Wavelength Radiometer[1]

GLENN E. SHAW

Geophysical Institute, University of Alaska, College

JOHN A. REAGAN

Department of Electrical Engineering, University of Arizona, Tucson

BENJAMIN M. HERMAN

Institute of Atmospheric Physics, University of Arizona, Tucson

(Manuscript received 25 July 1972, in revised form 6 November 1972)

ABSTRACT

A multiple wavelength solar radiometer designed for the purpose of measuring atmospheric optical depth at discrete wavelengths through the visible region is described. Experimental techniques, including sample observations, are presented for obtaining atmospheric optical depth from radiometer measurements. These techniques apply for conditions where the optical depth is either temporally variant or invariant during the course of a day. The influence of the aerosol size distribution on optical depth is investigated. Theoretical calculations of the wavelength dependency of the aerosol optical depth contribution are presented for several representative aerosol size distributions. Methods are also presented for estimating the aerosol size distribution and aerosol mass loading from multi-wavelength optical depth measurements.

1. Introduction

The purpose of this paper is to describe the design features and operational capabilities of a filter-wheel radiometer which has been employed on a nearly continuous basis for over a year to monitor atmospheric optical depth in Tucson, Ariz., at several wavelengths spaced throughout the visible region. As discussed in later sections of the paper, regular optical depth measurements not only provide baseline measurements of atmospheric turbidity, but also supply information from which useful estimates of aerosol mass loading may be made.

In addition to yielding optical depths, the radiometer output may also be related to the spectral characteristics of the zero airmass solar radiation. This affords an opportunity to check against zero airmass measurements obtained from aircraft and satellite observations. Furthermore, it is possible to utilize the zero airmass radiometer output to calibrate the radiometer in an absolute sense. The calibration procedure makes the instrument particularly useful for applications where the determination of radiant fluxes in absolute units is desired as well as providing a means for following temporal variations in optical depth, through the course of a day.

2. Description of filter-wheel radiometer

The basic requirement of the radiometer is to provide accurate measurements of the relative flux of directly transmitted sunlight received at the earth's surface as a function of zenith angle for selected wavelengths. Radiant energy within certain selected wavelength intervals is isolated by transmission through relatively narrow-band interference filters arranged in a rotating filter wheel. A second filter wheel containing neutral density filters of different opacities is included in the optical path of the system for the purpose of testing, calibration, and gain selection. After passing through the filters, the radiant energy is detected by a photodiode and converted to an electrical signal. The incident flux is also mechanically chopped to improve the signal level with respect to the dc component of the photodiode leakage current. A schematic illustration of the optical train of the radiometer is shown in Fig. 1.

The primary filter wheel of the radiometer contains eight interference filters which are spaced more or less uniformly in the visible region between 0.4 and 0.8 μm. All filters have been selected to avoid absorption lines and have passbands of about 0.1 μm which is sufficiently narrow so that little variation in flux occurs over the

[1] The research reported in this article has been supported by the Atmospheric Sciences Section of the National Science Foundation, under Grant GA-16764, and by the National Aeronautics and Space Administration, under Grant NGR 03-002-155, at The University of Arizona.

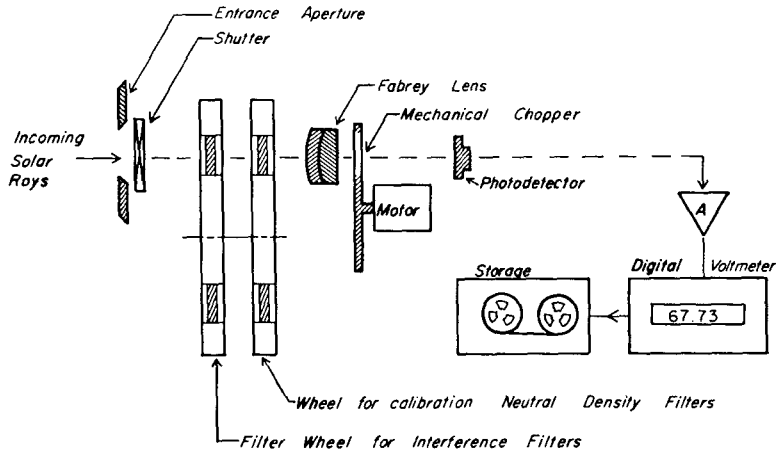

FIG. 1. Schematic illustration of the optical train for the multiple wavelength radiometer.

passband for continuous sources such as an incandescent filament or solar radiation. For these cases, the solar radiometer signal readings may be considered to be representative of fluxes evaluated at the center wavelengths of the filters.

Sequencing of the filters is accomplished by rotating the filter wheel with a dc drive motor which is actuated by a tab and micro-switch arrangement placed around the edge of the filter wheel. The switching arrangement and control circuitry are designed so that the filters are sequentially positioned into the optical path of the radiometer for 5-sec averaging periods. A cycle time of about 3 min is required to sequence through all the filters and repeat a measurement for a given wavelength. Output signals as well as coding signals to identify filter number are sampled and digitized by a digital voltmeter, and the voltmeter output is recorded with a paper tape printer. The entire system is automated to the extent that the radiometer may be left unattended for extended periods throughout the day.

Solar tracking is accomplished with a passive tracking equatorial mount which rotates at the siderial rate so that the radiometer remains pointed toward the sun as the earth rotates. The tracking error accumulated during the course of a day with this system (typically $<0.2°$ day^{-1}) is insignificant compared to the 3° field of view of the radiometer.

3. Determination of atmospheric optical depth with radiometer system

The filter-wheel radiometer has been employed on a nearly continuous basis for more than one year to monitor the ground-level direct solar radiation. The data so acquired have been related to optical depths of the atmosphere and signal levels which would correspond to the incident solar radiation at zero airmass. Of particular concern for this study was the determination of the aerosol particle contributions to the total optical depth.

Monochromatic direct solar radiation is related quantitatively to zero airmass, incident solar radiation by the Lambert-Beer law which may be expressed as

$$F(\lambda,z)=\left(\frac{r_m}{r}\right)^2 F_0(\lambda)\exp[-m(z)\tau_t(\lambda)]+F_d(\lambda,z), \quad (1)$$

where:

$F(\lambda,z)$	observed ground level solar flux at wavelength λ (W μm^{-1})
λ	wavelength (μm)
z	solar zenith angle
r	earth-sun distance at time of observation
r_m	mean earth-sun distance
$F_0(\lambda)$	zero airmass, directly transmitted solar flux at wavelength λ and at mean earth-sun distance (W μm^{-1})
$m(z)$	atmospheric airmass relative to the vertical direction
$\tau_t(\lambda)$	total optical depth at wavelength λ along the local zenith
$F_d(\lambda,z)$	diffusely scattered flux at wavelength λ entering radiometer (W μm^{-1}).

Complete solutions to the equations of radiation transfer including multiple scattering (Herman *et al.*, 1971) indicate that for model atmospheres with total optical depths up to $\tau_t=0.5$, the diffuse flux F_d contributes less than 2% to the total observed direct radiation for the 3° field of view of the radiometer so long as readings are not made for solar zenith angles $\gtrsim 80°$. The airmass factor $m(z)$ in Eq. (1) is approximately equal to sec$z$, but a more complete expression exists for $z>80°$ to take into account the curvature of the atmospheric layers and refraction effects caused by variations in the atmospheric densities (Rozenburg, 1966; Kondratiev, 1969).

The total optical depth $\tau_t(\lambda)$ results from a combina-

tion of effects which are illustrated mathematically by

$$\tau_t(\lambda) = \tau_R(\lambda)\frac{P}{P_0} + \tau_a(\lambda) + \tau_p(\lambda), \quad (2)$$

where:

- $\tau_R(\lambda)$ Rayleigh or molecular scattering optical depth for a standard atmosphere (Elterman, 1968)
- P atmospheric pressure at observer's site
- P_0 atmospheric pressure at sea level for a standard atmosphere
- $\tau_a(\lambda)$ optical depth arising from absorption by atmospheric gases such as ozone, water vapor, carbon dioxide, oxygen, etc.
- $\tau_p(\lambda)$ optical depth resulting from scattering and absorption by airborne atmospheric particulates contained in the air.

Determination of $\tau_t(\lambda)$ is accomplished by curve-fitting the radiometer measurements to Eq. (1) for the case where F_d is neglected, as has been previously done by Herman *et al.* (1971). This procedure is best illustrated by referring to the logarithmic form of Eq. (1), neglecting F_d, given by

$$\ln F(\lambda,z) = 2\ln(r_m/r) + \ln F_0(\lambda) - m(z)\tau_t(\lambda). \quad (3)$$

As the radiometer output voltage $V(\lambda,z)$ is linearly related to $F(\lambda,z)$, a plot of data points having ordinate values of $\ln V(\lambda,z)$ and abscissa values of $m(z)$ will, by Eq. (3), yield a linear curve of slope $-\tau_t$ so long as τ_t does not vary over the observation period. The total optical depth can then be determined by taking the slope of a straight line fitted to the data points. Moreover, the signal corresponding to zero atmospheric mass can be easily determined by extrapolating the straight line and noting its intercept on the ordinate. By comparing tabulated values of incident solar radiation at each filter wavelength to the extrapolated zero airmass signal, one can effect an absolute calibration of the system sensitivity in terms of signal per unit of incident radiant flux.

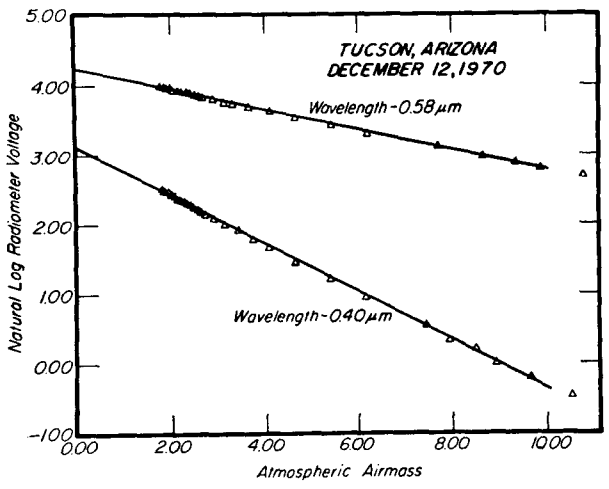

FIG. 2. Illustration of linear relation between log radiometer voltage and atmospheric airmass for data collected during clear stable atmospheric conditions.

Having determined the optical depth at each of the filter wavelengths λ_i, as outlined above, one may then proceed to derive the extinction which results from scattering and absorption by the atmospheric aerosols. Referring back to Eq. (2), this is done by calculating $\tau_R(\lambda_i)$, the optical depth due to scattering by air molecules, and $\tau_a(\lambda_i)$, the optical depth resulting from absorption, and subtracting these components from $\tau_t(\lambda_i)$. By carefully locating the central passband of the interference filters, one can often minimize or completely eliminate absorption effects from gaseous species such as water vapor and carbon dioxide, especially in the visible region where there are few significant absorption features. However, one must generally contend with the broad Chappius absorption bands of ozone since they extend over a considerable portion of the visible spectrum (from ~0.5–0.7 μm). Fortunately, the extinction due to ozone in the Chappius bands is fairly small and reasonably predictable so that the effects of ozone attenuation may be predicted with sufficient accuracy by referring to norms for columnar ozone amounts which are tabulated by latitude and season (Bates, 1954).

4. Utilization of solar radiometer for determining the time-dependent atmospheric transmission

The method of utilizing the filter-wheel radiometer for determining atmospheric optical depth as described above is dependent upon 1) having a linear response between output signal and input radiant energy, and 2) having the extinction properties of the atmosphere remain constant during the observations. The method of curve-fitting to derive $\tau_t(\lambda)$ does *not* depend on *a priori* knowledge of the absolute calibration constants for the radiometer. This is because the *slope* of a line drawn through the data points on a logarithmic signal voltage vs atmospheric airmass plot is used to calculate $\tau_t(\lambda)$, and *not* the absolute values of radiant flux. However, as previously mentioned, one can calibrate the filter-wheel radiometer in absolute units by referencing the extrapolated zero airmass signal to the known values for incident solar radiation (Thekaekara, 1970; Stair and Ellis, 1968).

Operationally, the zero airmass intercepts are determined for each wavelength by taking carefully controlled measurements of solar radiation during periods of constant and stable atmospheric extinction. The zero-airmass voltage intercept obtained from day to day should remain constant for clear stable days, and the mean value can be used along with values of tabulated incident solar flux to derive a calibration constant for the radiometer. Fig. 2 illustrates a Langley plot

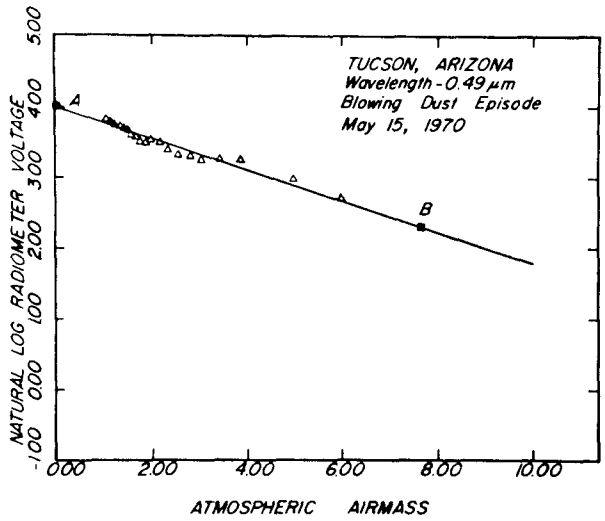

FIG. 3. Langley plot of solar radiometer data points for a blowing dust episode.

[$\log V$ vs $m(z)$] of data points at two wavelengths for measurements made at Tucson during very clear and stable conditions. As can be seen by inspecting the figure, the data points are arrayed in linear fashion in accordance with the functional form of the Lambert-Beer law given by Eq. (3). Intercepts corresponding to zero airmass found by extending the line drawn through the data points to the ordinate proved to be quite constant (typical variation of less than 3%) from day to day. The majority of the radiometer measurements yielded linear plots like those given in Fig. 2 so that it was possible to make accurate optical depth determinations from the slope of straight lines fitted to the data points on any individual day. For data points of the quality of those shown in Fig. 2, the rms error in the optical depth determination was typically less than 2%, while the corresponding error in the voltage intercept was typically less than 3%.

Whenever significant variations in atmospheric optical depth occurred during the course of a day, due to situations such as a frontal passage, blowing dust storm, pollution episode or the like, it was no longer possible to obtain optical depth by measuring the slope on a log V vs $m(z)$ plot. Data for an incident of this type are shown in Fig. 3 as a Langley plot collected during a blowing dust episode in Tucson. As indicated by the line in the plot from A to B, least-squares fitting of a line through the data points yields a quite ambiguous result for optical depth over the observation period. However, by using a previously determined value of the zero airmass intercept voltage (for a given wavelength), one can determine an "instantaneous" optical depth from the slope of a line drawn through the assumed zero airmass intercept voltage and the data point for a particular time. This method was employed to construct the curves given in Fig. 4 which describe the resultant time variation in optical depth evaluated at two wavelengths (one in the blue and the other in the red) for another blowing dust episode like the one noted above. It can be seen that the optical depth at each wavelength as well as the ratio of the two optical depths changed noticeably throughout the day. As discussed in the next section, the relationship between optical depths at various wavelengths can supply useful information about the aerosol size distribution.

5. Wavelength dependency of aerosol optical depth and its relation to aerosol size distributions and mass loading

The aerosol particle contribution to optical depth arises from the cumulative effects of scattering and absorption by the particulates distributed throughout the atmosphere. Assuming horizontal homogeneity, the aerosol optical depth component $\tau_p(\lambda)$ may be related to the extinction properties of the aerosol particles at any height h by

$$\tau_p(\lambda) = \int_0^\infty \beta(h,\lambda)dh, \tag{4}$$

where $\beta(h,\lambda)$ is the volume aerosol extinction coefficient at height h for wavelength λ. Furthermore, $\beta(h,\lambda)$ may be related to the aerosol size distribution which prevails at height h by

$$\beta(\lambda,h) = \int_{r_1}^{r_2} \psi(r,h)\sigma(\lambda,r,m)dr, \tag{5}$$

where:

r	aerosol particle radius
$\psi(r,h)$	aerosol size distribution at height h
$\sigma(\lambda,r,m)$	Mie single particle extinction cross section for a spherical particle of radius r, and index of refraction m which is illuminated by radiation of wavelength λ
r_1	minimum radius of particulates in sample
r_2	maximum radius of particulates in sample.

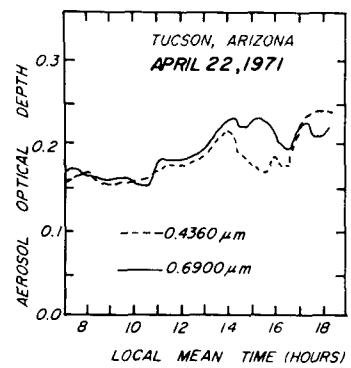

FIG. 4. Aerosol optical depth plotted as a function of local mean time for data acquired during a dusty period.

The aerosol particles are assumed to be spherical in shape, although it is known that both man-made and naturally occurring aerosols may be nonspherical. This assumption is essential because spherical particle theory (Mie, 1908) is the only tractable scattering theory which may be applied to the problem.

Direct sampling measurements of aerosols have revealed (Junge, 1963; Clark and Whitby, 1967) that the size spectrum of atmospheric aerosols can often be adequately described by a relationship known as the Junge distribution given by

$$\psi(r)=Cr^{-(\nu+1)}, \tag{6}$$

where C is a scaling constant directly proportional to the aerosol concentration, ν a shaping constant which normally is found to lie in the range $2\leqslant\nu\leqslant 4$, and $\psi(r)dr$ the number of particles per unit of volume with radii between limits r and $r+dr$. The distribution is typically assumed to apply over a size range extending from a lower limit of about $r=0.01\,\mu$m to an upper limit of about $r=10.0\,\mu$m.

Assuming the aerosol size distribution follows the Junge law given by Eq. (6), it can be shown that the extinction coefficient $\beta(\lambda,h)$, and hence $\tau_p(\lambda)$, has a wavelength dependency of the form (for example, see Bullrich, 1964)

$$\beta(\lambda,h)=k(h)\lambda^{-\nu+2}, \tag{7}$$

where k is a proportionality term dependent only on h, and ν is the shaping constant identified with Eq. (6). This expression is analytically true only if the aerosol size distribution extends over a sufficiently large radius range. Numerical evaluation of $\beta(\lambda,h)$ as given by Eq. (5) for the case where ψ follows the Junge distribution has shown that the expression for $\beta(\lambda,h)$ given by Eq. (7) is accurate to 2% for radii limits extending from $r=0.01$ to $10.0\,\mu$m and ν ranging from 2 to 4 (Shaw, 1971). These limits are representative of the limits typically applied to naturally occurring aerosols.

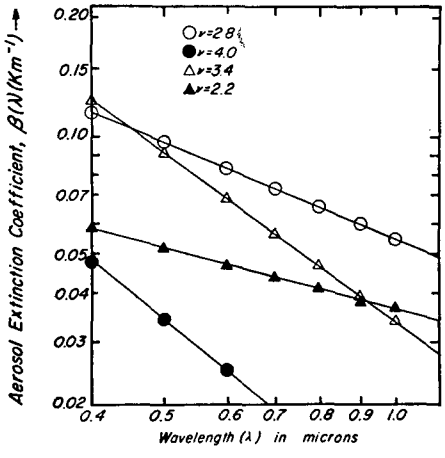

FIG. 5. Theoretically computed aerosol extinction coefficients plotted as a function of wavelength for selected values of the Junge constant ν.

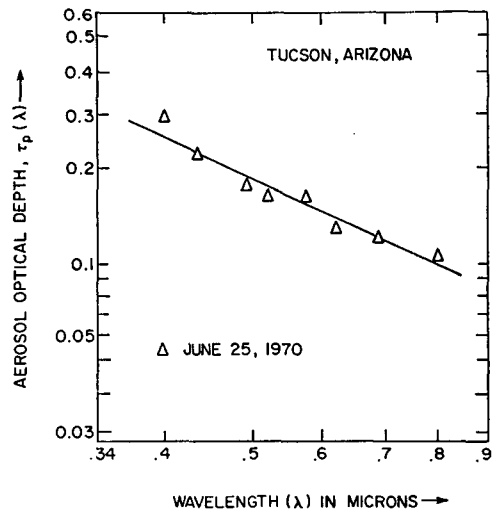

FIG. 6. Optical depth component due to aerosols as a function of wavelength.

FIG. 5 shows a series of curves that illustrate the variation of the extinction coefficient $\beta(\lambda,h)$ as a function of wavelength. The curves in Fig. 5 were calculated from the Mie theory for air containing aerosols distributed according to the Junge distribution, and all calculations were performed subject to the constraints of a real refractive index[2] of $m=1.54$, minimum and maximum radii limits of 0.01 and $10.0\,\mu$m, and a constant mass loading Γ of $200\,\mu$g m^{-3} of air. The different curves shown in the figure correspond to different values of the exponent ν in Eq. (6). The computed values of $\beta(\lambda,h)$ are plotted as a function of λ on a log-log scale and yield straight lines of slope $-\nu+2$ as would be expected from Eq. (7). It can be seen that $\beta(\lambda,h)$ may take on a wide range of values for any given wavelength, depending upon the value of the shaping constant ν.

By experimentally determining the optical depth due to aerosols, $\tau_p(\lambda)$, at several wavelengths, one can infer information regarding the aerosol size. For example, from the results given above regarding Eqs. (4)–(7), it is evident that one may determine the value of the shaping constant ν from $\tau_p(\lambda)$ so long as the aerosols are distributed, at least approximately, in the power law form expressed by Eq. (6). One can check whether the aerosol size distribution appears to follow the power law by plotting experimentally determined values of $\tau_p(\lambda)$ as a function of wavelength to compare against

[2] The aerosol refractive index is assumed to be equal to a real index of $m=1.54$ for all work presented in this paper. This value is typical of silicates, and one would assume that natural aerosols found in desert regions around Tucson would indeed have a large component of silicates. In addition, $m=1.54$ is quite close to the refractive indices of ammonium sulfate and sodium chloride, and these materials are also common constituents found in atmospheric aerosols (Junge, 1963). Finally, results of direct experimental measurements made by Hänel (1968) indicate that an index of about $m=1.54$ is apparently quite typical of a large class of atmospheric aerosols.

the wavelength dependency of Eq. (7). An example plot of this type is given in Fig. 6. The data points in the figure correspond to aerosol optical depths that were derived from total optical depth measurements made in Tucson with the solar radiometer (the rms error of each data point is estimated to be less than 2%). The figure has been plotted on a log-log scale so that the $\lambda^{-\nu+2}$ dependency given by Eq. (7), if obeyed, will manifest itself as a straight line. A least-squares fit of the data points yielded the solid line shown in the figure, and it can be seen that the expected straight line dependency is obeyed to a good approximation. The slope of the line fitted to the data points also yields as exponent ν for Eq. (7) of $\nu=3.32$.

Analysis of extinction data obtained with the filter-wheel solar radiometer at Tucson over a period of more than a year has indicated that the $\lambda^{-\nu+2}$ dependency of $\tau_p(\lambda)$ is sometimes, but by no means always, found. When the variation in $\tau_p(\lambda)$ does obey a power law, values of ν are found to range from about 2.4 to 4 with values mostly centered around $\nu\approx 3$. These values are in agreement with other studies of the size distribution for atmospheric aerosols (Junge, 1963; Clark and Whitby, 1967).

Besides being useful for inferring the size distribution of the atmospheric aerosols, the radiometer data can also be used to determine a numerical value for the total amount of particulate material contained in a column of unit area and extending vertically upward from the observer. However, the estimation of columnar mass loading is subject to several assumptions being valid. As previously mentioned, the assumption of a power law distribution can be substantiated, although not absolutely verified, by looking for a $\lambda^{-\nu+2}$ wavelength dependency of optical depth. When such a dependency is found, as was illustrated in Fig. 6, one may estimate the columnar mass loading in the following manner. First, the aerosol optical depth wavelength dependency, obtained from the multi-wavelength radiometer measurements, is used to determine the value of the size distribution exponent ν by slope fitting as described earlier. Having determined ν, the appropriate curve for that value of ν is located or extrapolated in Fig. 5, and the corresponding extinction coefficient value is read from the curve for a hypothetical air-sample containing 200 μg of aerosol loading per cubic meter. The actual value of mass loading M_L pertaining to the optical depth measurements may then be determined by employing a relation of the form

$$M_L=\Gamma_0\frac{\tau_p(\lambda_0)}{\beta(\lambda_0)}, \tag{8}$$

where:

M_L columnar mass loading of particulates over the observer (mass per unit area)

Γ_0 numerical value of aerosol mass loading constraint used for calculation of extinction coefficient in Fig. 5 (200 μg m^{-3})

$\tau_p(\lambda_0)$ particulate optical depth at a specific wavelength λ_0 (say $\lambda_0=0.50$ μm)

$\beta(\lambda_0)$ extinction coefficient or ordinate value of Fig. 5 evaluated at λ_0 for appropriate ν.

As an illustrative example of how the above-described technique may be employed, consider the experimentally determined aerosol optical depth vs wavelength dependency given earlier in Fig. 6. The slope of a straight line fitted to the data points in the curve yields, as given earlier, a value of ν of 3.32. Referring now to Fig. 5, there is a curve drawn for $\nu=3.4$. This curve is sufficiently close, as the accuracy to which ν can be determined from a typical set of optical depth data points (such as in Fig. 6) is about 5%. For $\nu=3.4$, $\beta_0(\lambda_0)$ is about 0.032 km^{-1} or 3.2×10^{-5} m^{-1} at $\lambda=0.5$ m, and (from Fig. 6) $\tau_p(\lambda)$ is about 0.18 at $\lambda=0.5$ μm. Substitution of these numerical values into Eq. (8) yields a value of columnar mass loading of 1.12 gm m^{-2}. Assuming the inferred value of ν to be accurate to within 5%, this yields a maximum uncertainty of about 20% in the mass loading.

No attempt was made in the above example to infer how the particulates were distributed with height. This is due to the fact that optical depth is an "integrated" parameter representative of the entire vertical atmosphere. While it is possible to infer limited information about the vertical aerosol distribution from slant-path attenuation measurements made very near the horizon, such inferences are subject to question, because the assumptions of horizontal homogeneity and negligible diffuse scattering are doubtful for the long atmospheric paths near the horizon. What would appear to be the most accurate method for remotely determining aerosol height distributions is to incorporate lidar measurements with the radiometer measurements. As recently discussed by Fernald *et al.* (1972), the important normalizing information supplied from optical depth measurements makes it possible, with certain assumptions, to determine the absolute values of the aerosol volume backscatter and attenuation coefficients as a function of height. With this information, along with the aerosol distribution obtained from multi-wavelength radiometer measurements, one could then infer the aerosol number density as a function of height.

6. Summary

The multiple wavelength radiometer described in this paper has been used successfully to study the extinction properties of atmospheric aerosols for atmospheric conditions where the optical depth is either temporally variant or invariant during the course of a day. Measurement of optical depth during periods of time-varying transmissivity require that the radiometer be absolutely calibrated, and a method has been given

whereby the radiometer may be so calibrated by employing the sun as a source. Studies have shown that it is quite easy to calibrate the radiometer at various wavelengths within a few percent by using the solar calibration technique, and such accuracy is quite compatible with what one could hope to achieve with present standard irradiance sources.

Data accumulated with the multiple wavelength radiometer have proven to be useful for deriving quantitative indices of atmospheric turbidity on a daily basis. The need for acquiring such information, on a large scale, has been dramatized in the last few years by expressed concern over possible climatic changes due to increased aerosol loading in the atmosphere (Rasool and Schneider, 1971) coupled with the apparent lack of available aerosol extinction data to quantitatively assess such concerns. While a great deal of pyrheliometer data have been collected, it is of limited value because it does not permit determination of the wavelength dependency of aerosol extinction. The importance of acquiring optical depth as a function of wavelength has been illustrated here by the presentation of calculations which demonstrated how greatly the aerosol optical depth vs wavelength relationship may change with variations in the aerosol size distribution. Moreover, methods have also been given which permit estimation of the aerosol size distribution and total mass loading once the wavelength dependency of the aerosol optical depth is known. As a final point, the authors therefore hope that this paper may serve in some sense to promote increased observations of optical depth as a function of wavelength around the world. Up-to-date optical depth data for Tucson, resulting from the study described here, will be published in the near future.

REFERENCES

Bates, D. R., 1954: The physics of the upper atmosphere. *The Solar System*, Vol. 2, G. P. Kuiper and B. M. Middlehurst, Eds., The University of Chicago Press, 576–643.

Bullrich, K., 1964: Scattered radiation in the atmosphere. *Advances in Geophysics*, H. E. Landsberg and J. Van Mieghem, Eds., Vol. 10, New York, Academic Press, 117–124.

Clark, W., and K. Whitby, 1967: Concentration and size distribution measurements of atmospheric aerosols and a test of the theory of self-preserving size distributions. *J. Atmos. Sci.*, **24**, 677–687.

Dave, J. V., 1968: Subroutines for computing the parameters of the electromagnetic radiation scattered by a sphere. Rept. No. 328-3237, IBM Scientific Center, Palo Alto, Calif., 65. pp.

Elterman, L., 1968: UV, visible, and IR attenuation for altitudes to 50 km, 1968. Rept. AFCRL-68-0153, Air Force Cambridge Research Laboratories, Bedford, Mass., 49 pp.

Fernald, F. G., B. M. Herman and J. A. Reagan, 1972: Determination of aerosol height distributions by lidar. *J. Appl. Meteor.*, **11**, 482–489.

Freidlander, S. K., 1961: Theoretical considerations for the particle size spectrum of the stratospheric aerosol. *J. Meteor.*, **18**, 753–759.

Hänel, G., 1968: The real part of the mean complex refractive index and the mean density of samples of atmospheric aerosol particles. *Tellus*, **20**, 371–379.

Herman, B. M., S. R. Browning and R. J. Curran, 1971: The effect of atmospheric aerosols on scattered sunlight. *J. Atmos. Sci.*, **28**, 419–428.

Junge, C. E., 1963: *Air Chemistry and Radioactivity*. New York, Academic Press, 383 pp.

Kondratiev, K. Ya., 1969: *Radiation in the Atmosphere*. New York, Academic Press, 912 pp.

Mie, G., 1908: Beiträge zur Optik Trüber Medien. *Ann. Phys.*, **25**, 377–445.

Quenzel, H., 1970: Determinations of size distributions of atmospheric aerosol particles from spectral solar radiation measurements. *J. Geophys. Res.*, **75**, 2915–2921.

Rasool, S. I., and S. H. Schneider, 1971: Atmospheric carbon dioxide and aerosols: Effects of large increases on global climate. *Science*, **173**, 138–141.

Rozenburg, G. V., 1966: *Twilight; a Study in Atmospheric Optics*. New York, Plenum Press (translated from Russian), 358 pp.

Shaw, G. E., 1971: An experimental study of atmospheric turbidity using radiometric techniques. Ph.D. dissertation, University of Arizona, 182 pp.

Stair, R., and H. T. Ellis, 1968: The solar constant based on new spectral irradiance data from 310 to 530 nanometers. *J. Appl. Meteor.*, **7**, 635–644.

Thekaekara, M. P., 1970: The solar constant and the solar spectrum measured from a research aircraft. NASA Tech. Rept. R-351, Goddard Space Flight Center, Greenbelt, Md., 85 pp.

van de Hulst, H. C., 1957: *Light Scattering by Small Particles*. New York, Wiley, 407 pp.

Yamamoto, G., and M. Tanaka, 1969: Determination of aerosol size distributions from spectral attenuation measurements. *Appl. Opt.*, **8**, 447–453.